Connectivity and topology of a phase-separating bicontinuous structure in a polymer mixture: Direct measurements of coordination number, inter-junction distances and Euler characte...

ARTICLE *in* THE JOURNAL OF CHEMICAL PHYSICS · OCTOBER 2003

Impact Factor: 2.95 · DOI: 10.1063/1.1607912

4 AUTHORS, INCLUDING:

Hiroshi Jinnai
Tohoku University
234 PUBLICATIONS **4,233** CITATIONS

SEE PROFILE

Connectivity and topology of a phase-separating bicontinuous structure in a polymer mixture: Direct measurements of coordination number, inter-junction distances and Euler characteristic

Hiroshi Jinnai,[a] Hideyuki Watashiba, Takashi Kajihara, and Masaoki Takahashi
Department of Polymer Science and Engineering, Kyoto Institute of Technology, Kyoto 606-8585, Japan

(Received 4 December 2002; accepted 17 July 2003)

A new set of topological parameters describing connectivity of a phase-separated bicontinuous structure of a polymer mixture in the late stage of spinodal decomposition has been *directly* measured by use of laser scanning confocal microscopy. A 3D thinning algorithm was used to transform one of the phase-separated domains into a skeletal network that locates at about the center of the domain. Number of channels intersecting at a junction, N_j, and distance between the adjacent junctions, D_j, were obtained from the resulting skeletal network. It was found that the phase-separated domain of the polymer mixture possesses, for the most part, 3 branches at each junction. The Euler characteristic, describing topology of the network, was found to be between ~ -2 to -4, topologically equivalent to a sphere with ~ 2 to 3 handles. Time-evolution of the histograms of the coordination number, $H(N_j)$, and distance, $H(D_j)$, clearly demonstrates that the bicontinuous structure grows with self-similarity in topological sense. © *2003 American Institute of Physics.* [DOI: 10.1063/1.1607912]

I. INTRODUCTION

The pattern formation and dynamics during the spinodal decomposition (SD) of binary mixtures are the fundamental problem of nonlinear, nonequilibrium phenomena. From industrial viewpoint, the problem is significant because the physical and mechanical properties of such systems are highly dependent on their high-order structures. Structural parameters characterizing global aspects of the phase-separating structures are quantitatively obtained by various scattering methods:[1] The global shape and periodicity of the structure can be characterized by the structure factor, $S(q,t)$, and by the dominant Fourier mode of the concentration fluctuations, $\Lambda(t)$, respectively (q and t are the magnitude of the wave vector and time, respectively).

Until recently, little attention has been paid to the local features of the phase-separating structure, e.g., interfacial shape and its dynamics, in spite of their apparent importance as a main driving force of the phase separation in the late stage SD; Minimization of the interfacial free energy of the system and hence to decrease the interfacial area is essential. Determination of the interfacial shape and its time-evolution are requisite, which became available only recently by three-dimensional (3D) microscopy, i.e., laser scanning confocal microscopy (LSCM).[2,3] Time-evolution of interfacial curvature distributions, $P(H,K;t)$ (H and K are the mean and Gaussian curvatures), was evaluated on the basis of the differential geometry to investigate the stability of the interface during SD.[4]

Although the basic kinetics of the SD processes can be understood by $S(q,t)$ and $\Lambda(t)$, these structural parameters do not seem to correlate *directly* with mechanical strength of materials. In contrast, the connectivity of the network and mechanical properties of the materials might be mutually related; In the medical science, the connectivity of trabecular bone attracts increasing attention, as it has been hypothesized that a loss of trabecular elements and consequently a loss in connectivity is primarily a reason for decreasing strength and stiffness in osteoporosis.[5] Establishing a methodology to measure the connectivity of various morphologies is a first question to be settled. An actual utility of the connectivity parameter(s) with respect to the mechanical strength will follow. Needless to say, the knowledge about the correlation between the morphology and mechanical strength should provide guideline for material design with superior mechanical strength in an effective way.[6] In addition, a scaling law for the connectivity has recently been proposed in a 3D system of the nonconserved order parameter by using simulation work based on the time-dependent Ginzburg–Landau (TDGL) equation.[7] In this article, it is also shown that the connectivity is a very sensitive measure to the occurrence of morphological transition.[8]

In the present paper, the connectivity of the bicontinuous structures of a polymer mixture in the late stage of SD was studied by thinning one of the domains and analyzing the resultant skeletal network structure. Two kinds of geometrical parameters characterizing the network connectivity, a number of channels intersecting at a junction (''channel coordination number''), N_j, and a distance between the adjacent junctions (''inter-junction distance''), D_j, were measured. Topological aspects of the phase-separated structures are examined by the Euler–Poincaré characteristic, χ, and genus, g, describing the complexity of the network domains.[9] Time-evolutions of those geometrical parameters were further used to test the validity of the dynamical scaling hypothesis in the late stage SD of the binary polymer blend.

[a]Electronic mail: hjinnai@ipc.kit.ac.jp

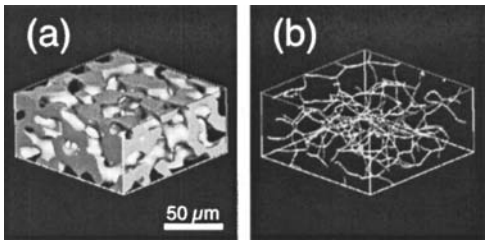

FIG. 1. (a) 3D LSCM image of DPB/PB mixture phase-separated for 2880 min after the onset of SD at 40 °C. The image shows only PB-rich domain and the DPB-rich domain is left empty. (b) Skeletal network corresponding to the same volume shown in part (a) after thinning of the PB-rich domain. Bar shows 50 μm.

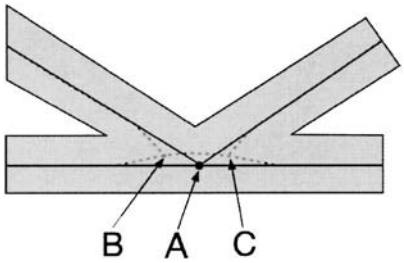

FIG. 2. Schematic of network strand (dashed line) after the 3D thinning of the precursor domain shown by gray area. Ideal skeletal network is shown by the solid line.

II. EXPERIMENT

A binary mixture of deuterated polybutadiene (DPB) and polybutadiene (PB) was used. The weight-average molecular weight (M_w) and polydispersity (M_w/M_n) of DPB were, respectively, 14.3×10^3 and 1.12 (M_n denotes the number-average molecular weight). M_w and M_w/M_n for PB were 9.5×10^3 and 1.07, respectively. The composition of the DPB/PB mixture, i.e., DPB/PB=46/54 vol%, corresponds to the critical composition according to the Flory–Huggins theory.[10] The mixture of DPB and PB was dissolved in benzene to form ~7 wt% solution and then lyophilized. The mixture after lyophilization was homogenized by the mechanical mixing[11] and placed between coverslips with a ring spacer whose thickness was 0.2–0.5 mm. The DPB/PB mixture was then heated to 40 °C to induce SD.

The phase-separated structures for six different phase-separation time intervals, all in the late stage of SD, were observed at room temperature by LSCM (Carl Zeiss, LSM410). Note that small amount of anthracene was attached to PB for contrast enhancement for LSCM. Two-dimensional (2D) optical slices with small depth of focus (~1 μm) were taken as a function of depth. The 2D images, binarized to find interface between the DPB-rich and PB-rich domains, were reconstructed into 3D images according to the protocol proposed by Lorensen *et al.*[12] The experimental setup and the reconstruction are detailed elsewhere.[4]

III. RESULTS

Figure 1(a) displays a 3D reconstructed image of the DPB/PB mixture phase-separated at 40 °C for 2880 min. The channel corresponds to the PB-rich domain, while the DPB-rich domain is transparent. The two domains are not intersecting and form 3D maze with an average periodicity of $\Lambda\cong19.2$ μm. The PB-rich domain was subjected to a 3D thinning algorithm originally proposed by Saito and Toriwaki[13] and Toriwaki and Mori[14] and modified by us to offer reliable measurements of network-type structures.[15] The algorithm was used to translate the volume image of the complex domain network into skeletal one. It uses the Euclidean distance transformation[16] to assure that each skeletonized network strand locates at the center of its precursor channel. The main modifications are the following: (i) We exclude junctions attached to the edge planes of the experimental volume data from statistical treatment, and (ii) avoid splitting a single junction into multiple junctions. The item (ii) would happen when the precursor networks merge at the junction with small angles as schematically shown in Fig. 2. Due to the Euclidean distance transformation, every point on the resultant skeletal network tried to keep equal distance from the interface, which, as a result, makes the network strand bend a little bit as illustrated by dashed lines in Fig. 2. Consequently, the true junction that should locate at a position "A" would split into two junctions labeled by "B" and "C" [see Fig. 2]. This problem is more pronounced as the number of network emerging from a single junction increases. In order to get around the split of the junction, a length parameter, L, is introduced: if the multiple junctions are found within a distance defined by L, one of the candidates (e.g., junctions "B" and "C" in Fig. 2) is assigned to a representative junction according to a certain rule.[17]

The periodic network structures with known N_j and D_j, e.g., the infinite periodic minimal surfaces (IPMS), were employed to confirm the accuracy of the 3D thinning algorithm. Various types of IPMS, such as the Schoen's gyroid (G) ($N_j=3$), diamond ($N_j=4$), I-WP ($N_j=8$), P ($N_j=6$) and neovius ($N_j=4$ and 12), were used.[15,18] It was found that our 3D thinning algorithm gave accurate measurements for N_j and D_j, as long as (i) there are enough number of unit cells ($C_{\text{total}}\geqslant100$, C_{total}: total number of the unit cell) in the 3D volume, (ii) the unit cell edge consists of more than 20 pixels, and (iii) L is set to be an averaged value of half the thickness of the precursor domain. The Euler–Poincaré characteristic, χ, and the genus, g (both described later below in Sec. IV A), topological measures characterizing the complexity of a network, can be accurately determined within ~10% error (e.g., the G morphology has $\chi=-8$ and $g=5$). Note that the condition (iii) was not actually important for the simple network morphologies with $N_j=3$ or 4 (G and diamond) to obtain quantitative results. (In other words, the split of the junction was not critical.)

Figure 3 demonstrates the spatial arrangements of the network strand with respect to the precursor bicontinuous domains. Figures 3(a)–3(d) show the results of the G morphology and Figs. 3(e)–3(h) correspond to the results of the DPB/PB mixture phase-separated at 40 °C for 1675 min. Thinning was carried out in the PB-rich domain. The solid line and the solid body in each 3D volume represent, respectively, the network strand and the DPB domain for the case of the DPB/PB mixture. It is clearly observed that the skeletal network computed by the 3D thinning locates at the

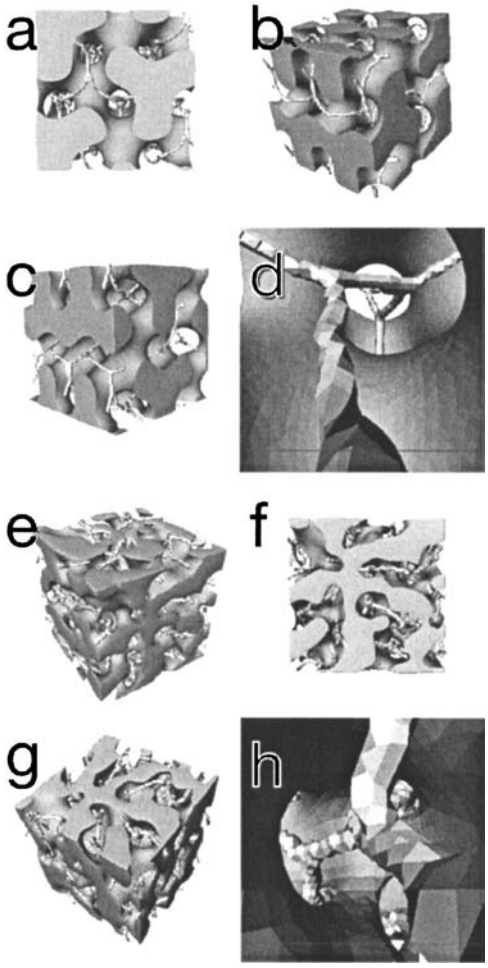

FIG. 3. Skeletal network after the 3D thinning of G morphology [(a)–(d)] and PB-rich domain the DPB/PB mixture [(e)–(h)]. G morphologies with the skeletal network from different view points are presented in (a)–(c). Similarly, (e)–(g) show DPB-rich network by solid body together with the network strand obtained from thinning the PB-rich domain from various angles. (d) and (h) demonstrate the network strand inside the 3D volume data for the G morphology and for the DPB/PB mixture, respectively.

center of the PB-rich domain. In addition, Figs. 3(d) and 3(h) show the skeletal network inside the 3D volume data for the G morphology and for the DPB/PB mixture, respectively. The network strand of the G morphology had 3-branched junctions as expected [see Fig. 3(d)]. More interestingly, there also existed 3-branched junctions in the DPB/PB mixture as demonstrated in Fig. 3(h).

TABLE I. Various structural parameters obtained from 3D thinning method.

t(min)	$\Lambda(\mu\text{m})^{a}$	$N_j^3(\%)^{b}$	$N_j^4(\%)^{c}$	$N_{\text{cell}}(\Lambda^{-3})$
1350	8.85	88.0	10.7	2.4
1675	11.5	85.7	11.7	2.0
2880	19.2	85.4	11.3	1.8
4610	31.4	73.9	16.5	2.0
7365	47.2	81.7	15.0	2.6
8610	62.8	83.9	8.7	1.2 ± 0.5

[a]Periodic length of phase-separating SD structure.
[b]Number of junctions having coordination number 3.
[c]Number of junctions having coordination number 4.

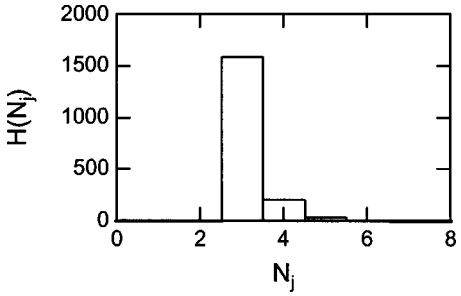

FIG. 4. Histogram of number of channels intersecting at a junction, $H(N_j)$, for the DPB/PB polymer mixture annealed at 40 °C for 2880 min. Percentages of 3- and 4-branches are 85.4% and 11.3%, respectively.

Depicted in Fig. 1(b) is the skeletal network after the 3D thinning of the PB-rich domain of the bicontinuous structure shown in Fig. 1(a). The topological parameters, N_j and D_j, were *directly* measured from this skeletal network. Two types of D_j were obtained: One represents the shortest distance between junctions, $D_{j,l}$ (“*linear distance*”) and the other corresponds to the distance measured along the skeletal network, $D_{j,p}$ (“*path distance*”). The subscripts l and p on D_j denote linear and path distances, respectively. Histograms of N_j, $H(N_j)$, and D_j, $H(D_j)$, were obtained by counting the channel coordination numbers at each junction and measuring the distance between the adjacent junctions. As noted above, if one of the network channels emerged from a junction attached to the edge planes of the experimental volume, it was excluded in the statistical treatment. This protocol is necessary to eliminate possible artifacts arising from thinning the domains at the edge plane where no information of the connectivity of the network to the outside of the measured volume is available.

Figure 4 shows $H(N_j)$ of the bicontinuous structure phase-separated at 40 °C for 2880 min [the same bicontinuous structure shown in Fig. 1(a)]. It was found that the bicontinuous structure possesses, for the most part, 3 branches at each junction (more than 85%). A coordination number of 4 accounts for 10% of the distribution measured in the SD bicontinuous morphology. The ratio of the junctions with different coordination numbers was, more or less, constant over the entire time range of our experiments. The percentages of the 3- and 4-branches are listed in Table I.

Demonstrated in Fig. 5 is $H(D_j)$ for the bicontinuous structure shown in Fig. 1(a). $H(D_{j,l})$ [Fig. 5(a)] and $H(D_{j,p})$ [Fig. 5(b)] are shown. Common features between the obtained two kinds of distributions are evident: The histograms showed shoulder-like broad maximum at $D_{j,l}\sim13\ \mu$m and $D_{j,p}\sim15\ \mu$m ($D_{j,l}/\Lambda\sim0.68$ and $D_{j,p}/\Lambda\sim0.78$). In addition, the phase-separated structure consists of junctions separated by surprisingly short distances (~0.1 to $0.2\ \Lambda$). No significant difference between the distributions between $D_{j,l}$ and $D_{j,p}$ is observed, indicating that the domains are not tightly curved or winding. Although D_j had broad distribution, the maximum positions of $D_{j,l}$ and $D_{j,p}$ are similar to the periodicity of the bicontinuous structure, i.e., 19.2 μm and thus these number seems to be related to Λ. In fact, the nano-scale bicontinuous structure of a poly(styrene-*b*-isoprene-*b*-styrene) (SIS) triblock copolymer, similar in N_j

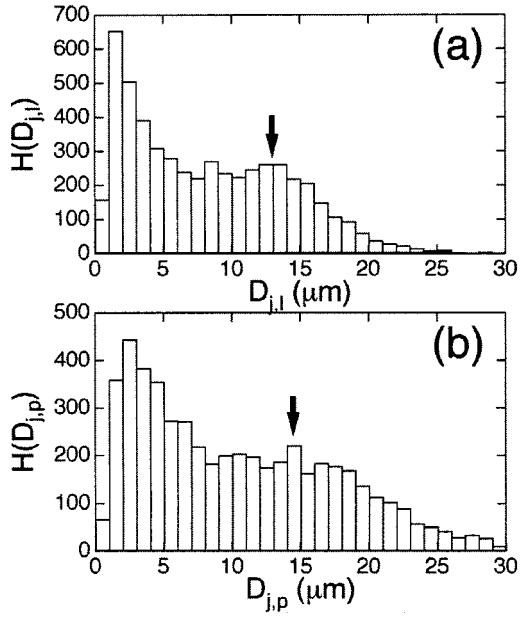

FIG. 5. Histograms of straight distance, $H(D_{j,l})$ (a), and path distances, $H(D_{j,p})$ (b), for the DPB/PB polymer mixture annealed at 40 °C for 2880 min. The linear distance corresponds to the shortest distance between the junctions, and the path distance to the distance along the skeletal network, respectively. There are substantial short distances in both histograms. Arrows in (a) and (b) indicate peak distances in each histogram.

but different in size, exhibited *sharp* maximum at $D_j/\Lambda \sim 0.4$ (Ref. 19) (see Fig. 3 in Ref. 20).[21] Detailed crystallographic analysis on the SIS triblock copolymer yielded that it has $Ia\bar{3}d$ symmetry (G morphology). The relation, $D_j/\Lambda \sim 0.4$, is a prediction of the G morphology and thus the maximum in $H(D_j)$ is surly related to Λ.

N_{cell} reflecting the density of the junctions of the network structure, can be estimated from the total number of junctions, N, in the measured volume, knowing the volume of the unit cell. The DPB/PB blend at $t=2880$ min exhibits $N_{\mathrm{cell}}=1.8$, where Λ is taken as the edge of the unit cell. The experimentally obtained N_{cell} was more or less constant (average value: $\bar{N}_{\mathrm{cell}}\sim 2.0$) over the entire time range of our experiment as shown in Table I.

IV. DISCUSSIONS

A. Comparison of SD morphology with mathematical model

As depicted in Fig. 4, the dominant N_j is 3 for the phase-separated structure of the DPB/PB mixture. Having the IPMS, e.g., G morphology (G morphology has 3 branches at each junction), as a model network structure to the bicontinuous structure would be justified since they are a series of mathematically predicted structures with least surface area under certain boundary condition: Dominant driving force for the polymer mixture to form phase-separating structure is to avoid contact between the dissimilar species due to the repulsive interaction between them and thus the interfacial area where the two polymers have contact should be minimized. The G morphology has $N_{\mathrm{cell}}=8$. $H(D_j)$ of the G morphology shows narrower distribution (peaked at 0.4 Λ) than that of the SD morphology of the DPB/PB mixture.

Interfacial area per unit cell volume, S_{cell}, was evaluated to be ~ 2.8 for the phase-separated structures of the DPB/PB mixture, while S_{cell} for the G morphology is 3.1. The unit is Λ^{-1}. It is intriguing that the interfacial area is smaller for the SD morphology than that for the G morphology. As the G morphology is a crystalline structure, junctions have to be three-dimensionally arranged so as to realize $Ia\bar{3}d$ space group. $S_{\mathrm{cell}}=3.1$ is achieved under such constraint. In contrast, the phase-separating structure of the DPB/PB polymer blend is free from such constraint and seemed to obtaine lower S_{cell} than the G morphology by sparsely and irregularly packing junctions in 3D space.

The Euler–Poincaré characteristic, χ, and the genus, g, can be estimated from the total number of junctions, N, and total number of branches, B, through the following equation:[22]

$$\chi_{\mathrm{skel}}=2N-B. \tag{1}$$

Here $B\equiv\Sigma_{i=1}^{N}N_{j,i}$ ($N_{j,i}$ is the coordination number at the ith junction). The Euler characteristic per unit cell volume, χ_{skel}, at various t was evaluated from Eq. (1) and listed in Table II. The Euler characteristic is alternatively obtained from the Gauss–Bonnet (GB) theorem:[9]

$$2\pi\chi_{\mathrm{GB}}=\langle K\rangle\cdot S. \tag{2}$$

Here $\langle K\rangle$ and S are an area-average Gaussian curvature and an interface area, respectively. The quantities used in the estimation of χ_{GB} are taken from Ref. 4. Note that this theorem assumes that the surface is closed, while there is no such requirement in Eq. (1). The theorem is important since it relates the local structural parameter, i.e., the Gaussian curvature, to the global one as characterized by χ. χ_{skel} spans from -1.6 to -3.0 over the time range of our experiments. Reasonable agreement between χ_{skel} and χ_{GB} are found, although χ_{GB} tends to be smaller than χ_{skel} at a given phase-separation time. This differences in χ between the two methods may be due to the statistical accuracy intrinsic to them. In the 3D thinning method, a large 3D volume is necessary in order to obtain enough numbers of N and B and hence the achievement of good statistics is normally difficult. In contrast, the Gauss–Bonnet theory uses the entire interfacial area contained in a 3D volume data. Hence, it usually offers better statistical accuracy than that from the 3D thinning for a given 3D volume.[15,23] Nevertheless, both χ_{skel} and χ_{GB} exhibited similar time-change: They are almost constant over the time scale of our experiments (average values: -2.4 and -3.6 for χ_{skel} and χ_{GB}, respectively) or slightly increased towards the end of the experiment. If the latter is what has happened, the increase in χ indicates the occurrence of breakup of bicontinuous network and hence decrease of connectivity during SD[24] (see also the following paragraph).

The genus is related to χ in the following way:[9] $g=1-\chi/2$. A surface with genus g is topologically equivalent to a sphere with g handles. For example, the bicontinuous structures of the DPB/PB mixture at $t=2880$ min exhibited $\chi_{\mathrm{skel}}\simeq -2.7$ ($\chi_{\mathrm{GB}}\simeq -4.0$) and hence $g_{\mathrm{skel}}\simeq 2.3$ ($g_{\mathrm{GB}}\simeq 3.0$).

TABLE II. Various structural parameters obtained from 3D thinning method.

t(min)	χ_{skel}[a]	g_{skel}[b]	χ_{GB}[c]	g_{GB}[d]	C_{total}[e]	B_{cell}[f]
1350	−2.95	2.47	−4.67	3.33	413.3	7.7
1675	−2.32	2.16	−3.79	2.89	1110.4	6.4
2880	−2.65	2.32	−3.98	2.99	479.4	6.2
4610	−2.18	2.68	−3.57	2.78	46.6	6.2
7365	−2.79	2.39	−3.57	2.79	25.8	8.0
8610	−1.57	1.78	−2.75	2.37	85.3	3.9

[a]The Euler–Poincaré characteristic per Λ^3 obtained from 3D thinning method.
[b]The genus per Λ^3 obtained from 3D thinning method.
[c]The Euler–Poincaré characteristic per Λ^3 obtained from the Gauss–Bonnet theory.
[d]The genus per Λ^3 obtained from the Gauss–Bonnet theory.
[e]Total number of unit cells($=\Lambda^3$) in the LSCM volume data used in the 3D thinning analysis.
[f]The total number of branches per Λ^3.

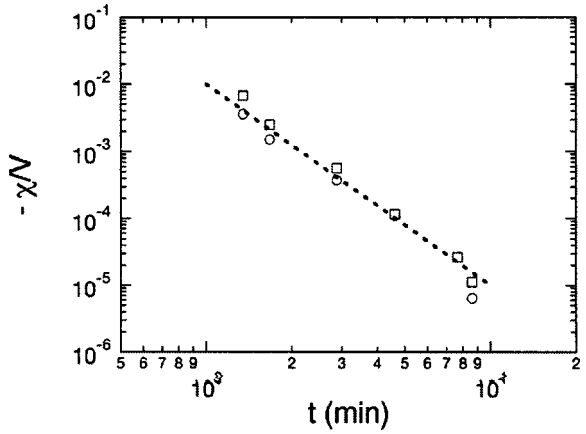

FIG. 7. A double logarithmic plot of topological parameter, $-\chi/V$ as a function of t. Two kinds of Euler numbers, $-\chi_{\text{skel}}/V$ (○) and $-\chi_{\text{GB}}/V$ (□), were estimated by Eqs. (1) and (2), respectively. Dotted line represents $-\chi/V \sim t^{-3}$.

The genus varied between 2 and 3 but showed no time-dependence or slight decrease towards the end of our experiment (see Table II). Thus, the bicontinuous SD morphology is topologically equivalent to a sphere with ~2 to 3 handles. Note that the G morphology is topologically equivalent to a sphere with five handles. Thus, the bicontinuous network structure of the DPB/PB mixture is less complex and loose network than that of the G morphology, 3-branched mathematically predicted model network structure.

B. Test of dynamical scaling hypothesis

It was shown in a number of scattering and microscope experiments that the bicontinuous structure evolves with dynamical self-similarity in the late stage of SD. In our previous study,[4] we demonstrated that the dynamical scaling law in terms of local structure, such as the interfacial shape, holds. In the present study, a test of the hypothesis in terms of the topology was carried out.

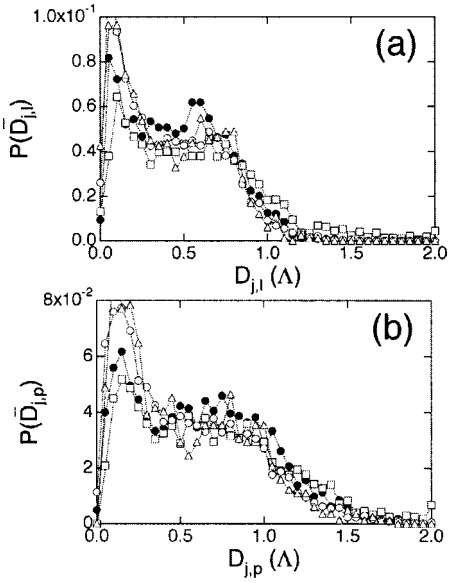

FIG. 6. Scaled probability densities (a) $P(\overline{D}_{j,l})$ and (b) $P(\overline{D}_{j,p})$ for the DPB/PB mixture in the late stage SD at four representative time: 1350 min. (●), 1675 min (□), 2880 min (○), and 8610 min (△).

First, the scaled probability densities of the two kinds of interjunction distances (both linear and path distances), $P(\overline{D}_{j,i}) \equiv \int H(\overline{D}_{j,i}) d\overline{D}_{j,i} = 1$ $[\overline{D}_{j,i} \equiv D_{j,i}/\Lambda$ $(i = l$ or $p)]$, at four representative phase-separation times are presented in Figs. 6(a) and 6(b). The scaled probability densities do not depend on the phase-separation time and fall onto master curves.[25]

Second, following the discussion given by Fiałkowski *et al.*,[7] the scaling hypothesis in terms of $\chi(t)$ was experimentally examined. The scaling laws for different morphological measures, such as $\chi(t)$ and an interfacial area per unit volume, $\Sigma(t)$, are given in the following way:

$$\chi(t) \sim \Lambda(t)^{-d}, \tag{3}$$

$$\Sigma(t) \sim \Lambda(t)^{-1}, \tag{4}$$

where d is the dimensionality of the system ($d=3$ in our case). We reported $\Lambda(t) \sim t^1$ and $\Sigma(t) \sim t^{-1}$ in our previous paper.[4] Thus, Eq. (4) has been already confirmed. In Fig. 7, the Euler numbers per volume estimated by two methods, i.e. Eqs. (1) and (2), were plotted against t in double-logarithmical way. It is clearly shown that $-\chi/V \sim t^{-3}$, in excellent agreement with the prediction given by Eq. (3). Therefore, it is evident (from Figs. 6 and 7) that the dynamical scaling hypothesis exclusively holds in the late stage of SD not only in local sense but also global, especially in topological, sense.

ACKNOWLEDGMENTS

The authors are grateful to Dr. Yukihiro Nishikawa for his help in data analysis. H.J. is partially supported by the Grant-in-Aid for Scientific Research on Priority Areas (A), ''Dynamic Control of Strongly Correlated Soft Materials'' (Nos. 413/13031057 and 14045246) from the

Ministry of Education, Science, Sports, Culture, and Technology. H.J. is grateful to NEDO for support of this research through a Japanese National Project ''Nano Structure Polymer Project'' by the Ministry of Economy, Trade and Industry.

[1] T. Hashimoto, in *Structure and Properties of Polymers*, edited by R. W. Cahn, P. Haasen, and E. J. Kramer (VCH, Weinheim, 1993), Vol. 12 of Materials Science and Technology, p. 251.
[2] H. Jinnai, Y. Nishikawa, T. Koga, and T. Hashimoto, Macromolecules **28**, 4782 (1995).
[3] H. Jinnai, T. Koga, Y. Nishikawa, and T. Hashimoto, Phys. Rev. Lett. **78**, 2248 (1997).
[4] H. Jinnai, Y. Nishikawa, H. Morimoto, T. Koga, and T. Hashimoto, Langmuir **16**, 4380 (2000).
[5] J. Kabel, A. Odgaard, B. van Rietbergen, and R. Huiskes, Bone **24**, 115 (1999).
[6] H. Jinnai, T. Kajihara, Y. Nishikawa, M. Ito, S. D. Smith, D. A. Agard, and R. J. Spontak, Adv. Mater. (Weinheim, Ger.) **14**, 1615 (2002).
[7] M. Fiałkowski, A. Aksimentiev, and R. Hołyst, Phys. Rev. Lett. **86**, 240 (2001).
[8] A. Aksimentiev, M. Fiałkowski, and R. Hołyst, Adv. Chem. Phys. **121**, 141 (2002).
[9] S. Hyde, S. Andersson, K. Larsson, Z. Blum, T. Landh, S. Lidin, and B. W. Niham, *THE LANGUAGE OF SHAPE* (Elsevier, Amsterdam-Lausanne-New York-Oxford-Shannon-Tokyo, 1997).
[10] P. J. Flory, *Principles of Polymer Chemistry* (Cornell University, New York, 1953).
[11] T. Hashimoto, T. Izumitani, and M. Takenaka, Macromolecules **22**, 2293 (1989).
[12] W. E. Lorensen and H. E. Cline, Comput. Graphics **21**, 163 (1987).
[13] T. Saito and J. Toriwaki, IEICE Trans. Inf. Syst. **E77-D**, 1005 (1994).
[14] J. Toriwaki and K. Mori, in *Digital and Image Geometry*, edited by G. Bertrand, A. Imiya, and R. Klette (Springer-Verlag, Berlin-Heidelberg, 2001), Vol. 2243 of LNCS, p. 412.
[15] Y. Nishikawa, H. Jinnai, and H. Hasegawa, Kobunshi Ronbunshu **58**, 13 (2000).
[16] T. Saito and J. Toriwaki, Pattern Recogn. **27**, 1551 (1994).
[17] If there are multiple candidate for a junction, we used the following rule to determine the position of the junction. (i) Take one of the multiple junctions and check the length of the branches (network strands emerging from the junction). If one of the branches of this junction (junction 1) is shorter than L, look at the adjacent junction (junction 2) attaching to this short branch. Check the length of the branches of the junction 2. If these two junctions share the same short branch and their other branches are longer than L, place a junction at the middle of the two junction (on the short branch). (ii) In the above rule, if the junction 2 has more than one short branches attached to it, junction 1 transfers its right as a junction to junction 2 (so that junction 1 is not a junction any more). Repeat the two conditions until a single junction can be found.
[18] Note that the resolution of the model is comparable to that of the 3D images of the DPB/PB phase-separating morphologies and thus the results can be directly applicable to the SD morphologies in the present study.
[19] H. Jinnai, Y. Nishikawa, R. J. Spontak, S. D. Smith, D. A. Agard, and T. Hashimoto, Phys. Rev. Lett. **84**, 518 (2000).
[20] H. Jinnai, T. Kajihara, H. Watashiba, Y. Nishikawa, and R. J. Spontak, Phys. Rev. E **64**, 010803(R) (2001).
[21] H. Jinnai, T. Kajihara, H. Watashiba, Y. Nishikawa, and R. J. Spontak, Phys. Rev. E **64**, 069903(E) (2001).
[22] S. T. Hyde and S. Ramsden, in *Discrete Mathematical Chemistry: DIMACS Workshop Discrete Mathematical Chemistry*, edited by P. Hansen, P. Fowler, and M. Zheng (American Mathematical Society, Providence, 2000), Vol. 51 of DIMACS Series in Discrete Mathematics and Theoretical Computer Science, p. 203.
[23] Agreement between χ_{skel} and χ_{GB} has been tested using various types of IPMS. We obtained reasonable agreement between the two methods, provided that there are enough number of unit cells ($C_{\mathrm{total}} \geqslant 100$, C_{total}: Total number of the unit cell) in the 3D volume. Namely, accuracy of χ_{skel} strongly depends on C_{total} and thus on N and B contained in the volume used for the measurements.
[24] H. Jinnai, H. Kitagishi, K. Hamano, Y. Nishikawa, and M. Takahashi, Phys. Rev. E **67**, 021801 (2003).
[25] Although the scaled probability densities of the interjunction distances did not exhibit appreciable time-change, the slight increase of χ (or decrease of g) was observed. This might be an indication of an onset of a topological change of the phase-separated structure due to propagation of cylindrical domains, induced by preferential wetting of PB domains to glass surface, into the interior portion of the sample (Ref. 24). At $t > 8000$ min, both N_{cell} and B decreased.